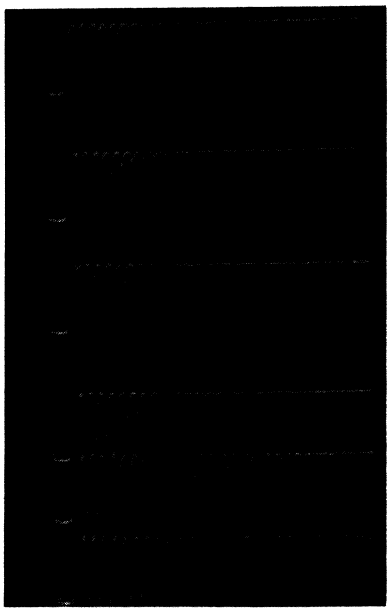

FIG. 2. Changes in the pulse amplitude (at 25 Mc) as a function of time, or distance in the material, at the magnetic field intensities of Fig. 1. The top trace is that with zero applied magnetic field, and the bottom trace is that with saturation field.

Similar effects have been observed in iron-silicon single crystals (3.8 percent Si) but the magnitude of the effect is much smaller. Cobalt has not been examined.

Although the equipment used is capable of detecting velocity changes of less than 0.1 percent, no velocity changes were observed with applied magnetic field corresponding to the above attenuation changes.

Additional experiments with nickel have been made in which the applied magnetic field is directed along the axis of the ultrasonic beam. The result of these observations is that qualitatively the variations of attenuation with magnetic field follows the same pattern as that just described with the applied magnetic field perpendicular to the ultrasonic beam. In the latter case it does not make any appreciable difference what angular position the applied magnetic field has around the beam axis.

The effect of the magnetic field in orienting the magnetic moments appears to be directly coupled to the lattice in such a way that attenuation of the ultrasonic energy is reduced when a saturation field is applied. It may be that the large change observed is a change in the scattering of the ultrasonic radiation by the lattice which is affected by the magnetic domain orientations, hence by the applied magnetic field. It may also be that there are magnetic losses caused by induced currents within the domains—currents which might arise from the passage of a mechanical wave through a magnetostrictive medium. The remaining attenuation value at saturation is probably caused by the absorption of energy by the lattice because of work done on it. The ultrasonic waves were compressional, and the wavelength in the nickel varied from approximately 0.1 cm at 5 mc to 0.01 cm at 50 megacycles. The magnetic domain size in nickel falls within this range of wavelengths. Anisotropy properties of single crystals are being investigated by this method.

* The work described here was supported by the Research Corporation of New York and by the Office of Air Research.

[1] Ultrasonic attenuation is measured by a pulsed system using microsecond pulses with a 300 rep. rate. The attenuation values are free of any effects of boundary conditions or beam spreading, and are characteristic only of the material. Details of such measurements are described in a report entitled "On the measurement of ultrasonic attenuation in solids" by R. L. Roderick and R. Truell (to be published).

Correlation Phenomena and Capture of Polarized Neutrons

OTTO HALPERN
University of Southern California, Los Angeles, California
(Received June 14, 1951)

IN a recent note,[1] attention was called to the fact that the capture of a polarized neutron when followed by the emission of a single gamma-quantum leads to certain polarization effects in the final nucleus as well as in the emitted radiation. A special simple example was discussed, while the treatment of more complicated cases and the question of the design of a gamma-ray analyzer was left to a more detailed paper.

This transfer of polarization has considerable influence, also, in such cases in which the transition to the final state is carried out in two (or more) steps. One can here expect the occurrence of very significant changes in the theory of correlation. This may perhaps best be illustrated if we apply the statistical interpretation[2] of a general group-theoretical result[3] concerning correlation effects to the present case.

The absence of interference effects between the transition amplitudes to and from the intermediate state of the final nucleus was ascribed[2] to the fact that the projection of the angular momentum on the direction of propagation of the emitted quantum is a good quantum number provided that spatial degeneracy allows resolution of the angular momentum along any direction, and in particular, along the wave vector of an emitted particle. This condition no longer obtains if the initial state is formed through capture of a polarized neutron. Depending upon the angular momentum of the original nucleus, the initial state of the final nucleus is totally or partially polarized. The description of the process of emission is no longer invariant under rotation around the direction of propagation, since a preferred direction is established through the axis of polarization. Simple relations are again encountered if, e.g., the direction of emission of the quantum coincides with the axis of polarization of the incident neutron.

A quantitative discussion is reserved for a later publication.

[1] O. Halpern, Phys. Rev. **82**, 753 (1951).
[2] B. A. Lippmann, Phys. Rev. **81**, 162 (1951).
[3] S. P. Lloyd, Phys. Rev. **80**, 118 (1950).

On the Goldberger Model for the Interaction of High Energy Nucleons with Heavy Nuclei*

G. BERNARDINI, E. T. BOOTH, AND S. J. LINDENBAUM
Columbia University, New York, New York
(Received May 24, 1951)

GOLDBERGER[1] considered as a model for the inelastic interaction of 90-Mev neutrons with a heavy nucleus (Pb) the generation of an internal nucleonic cascade in a zero temperature Fermi gas of nucleons. The Monte Carlo method was employed to treat the cascades which were developed in accordance with free nucleon-nucleon scattering cross sections (appropriately reduced by the Pauli exclusion principle).

An experimental check of Goldberger's[1] evaluation by Hadley and York[2] was interpreted to be at best only in partial qualitative agreement. The discrepancies may have been due to the failure of the model at these low energies for which pick-up effects, multiple nucleon interactions, and refraction effects could be important. The use of erroneous cross sections ($p-p$, $n-n$) and some approximations in the calculations also are at least partially responsible for the discrepancy.

To check the model at higher energies (~400 Mev), the nuclear interactions induced by 350- to 400-Mev protons[3] in β-sensitive nuclear emulsions were compared to the model predictions. This technique is particularly well suited for this study, because all charged particles from the individual nuclear events are visible,

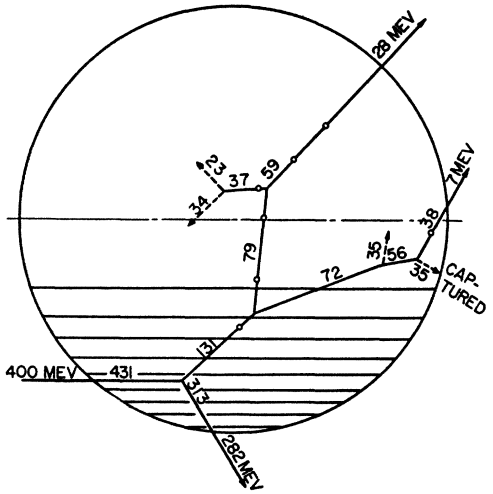

FIG. 1. A Goldberger model work diagram. Cross section of nucleus of mass number 100, using for the radius $R=1.4\times A^{\frac{1}{3}}\times 10^{-13}$ cm. Thermal excitation = 66 Mev.

and hence a detailed comparison with the calculations can be made. About 80 percent of the inelastic events in emulsions occur in Ag—Br nuclei of average mass number 100, and hence the calculations were performed for $A=100$.

A two-dimensional circular geometry ($R=1.4A^{\frac{1}{3}}\times 10^{-13}$ cm) was employed for the nucleus. The true three-dimensional location of the first interaction was preserved by dividing the two-dimensional circle into segments which when rotated present equal normal ring area to the incident nucleon (see Fig. 1). Equal numbers of nucleons were then considered incident upon each segment.

The individual properties of protons and neutrons were replaced by an average nucleon gas with a maximum kinetic energy of 22 Mev in a nuclear barrier (including coulomb) of 35 Mev. The average mean free path inside the nucleus as a function of energy was determined from published experimental $n-p$ and $p-p$ cross-section measurements, and the assumption $\sigma_{n-n}\approx\sigma_{p-p}$. The Monte Carlo calculations follow the general Goldberger technique, and a typical calculation is illustrated in Fig. 1. Of 90 incident nucleons only 60 produced inelastic events.

For a comparison with the experimental results the ejected nucleons were grouped into the energy intervals designated[3] as gray (>100 Mev), sparse black (30 to 100 Mev), and black (<30 Mev). The calculated two-dimensional angular distributions are compared with the experimental projected angular distributions in Fig. 2. The agreement is clearly reasonable within statistics and experimental errors in the values of prong energies.

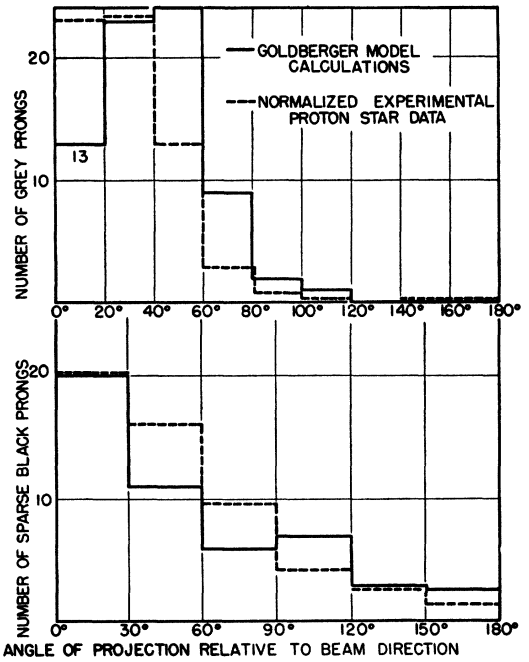

FIG. 2. A comparison of the Goldberger model angular distributions with the experimental proton star data.

An analysis of the calculations revealed that a reasonable estimate of the fraction of ejected nucleons which are protons is $\frac{1}{2}$.

The comparison of experimental and predicted mean prong numbers is made in Table I. The thermal excitation is calculated from the conservation-of-energy equation. The average value is 50 Mev and the maximum value about 200 Mev illustrating that the knock-ons carry away most of the incident energy.

The value of 35 Mev per black prong[4] was used to estimate the mean evaporation black prong number in Table I. This gave the correct (within the errors) total mean prong number as well as a percentage (28±7 percent) of knock-on black prongs which agrees with the experimental determination of at least 25 percent.

Table II is a comparison of the distribution of events with various numbers of gray protons (>100 Mev) and fast protons (<30 Mev). The agreement is clearly reasonable for this rather sensitive

TABLE I. Comparison of experimental and calculated mean prong numbers.

A. Gray and sparse black prongs

	Gray (>100 Mev)	Sparse black (30–100 Mev)
Calculated mean No. of protons	0.6 ±0.12	0.42 +0.1
Experimental mean No. of protons	0.42±0.04	0.35±0.04

B. Black prongs

	Black prongs (>30 Mev)
Calculated mean No. of directly ejected protons	0.58±0.12
Estimated mean No. of evaporation prongs	1.5 ±0.2
Estimated mean No. of visible black prongs	2.1 ±0.4
Experimental mean No. of black prongs	2.5 ±0.2

TABLE II. Comparison of experimental and calculated distribution of gray (>100 Mev) and fast (>30 Mev) proton events.

A. Gray proton events

No. of gray protons	% of events calculated	% of events experimental
0	46±11	57 ±4
1	48±11	40 ±4
2	7±4	2.5±1

B. Fast proton events

No. of fast protons	% of events calculated	% of events experimental
0	30±7	35 ±3
1	48±8	54 ±4
2	21±7	9 ±2
3	3±1.5	1.7±0.7

test of the cascade nature of the process. A detailed report to be published shortly will show that all the results of the 400-Mev proton interactions can be satisfactorily explained by the model.

A similar investigation at 150 Mev is now in progress.

The authors wish to thank Mr. Leon Landowitz and Mr. Jack Leitner for their excellent work on the Monte Carlo calculations.

* This project was jointly supported by the ONR and AEC.

[1] M. L. Goldberger, Phys. Rev. **74**, 1269 (1948).
[2] J. Hadley and F. York, Phys. Rev. **80**, 345 (1950).
[3] Bernardini, Booth, and Lindenbaum, Phys. Rev. **80**, 905 (1950).
[4] Bernardini, Cortini, and Manfredini, Phys. Rev. **79**, 952 (1950).

A Note on the U Operator*

MAURICE NEUMAN
Brookhaven National Laboratory, Upton, Long Island, New York
(Received June 8, 1951)

IT is usually assumed that the operator $U(t)$ transforming the state vector from the interaction to the Heisenberg representation satisfies the relation

$$\bar{U}(t)=U^{-1}(t), \tag{1}$$

where the dash denotes the hermitian adjoint. One then infers from Eq. (1) that

$$\bar{S}=S^{-1}. \tag{2}$$

Here

$$S=\lim_{t\to\infty}U(t). \tag{3}$$

It is the purpose of this note to show that Eq. (2) is implied by the formal structure of the theory; statement (1), however is not. Its use amounts to an additional assumption. The failure of (1) need not be related to convergence or renormalization difficulties

We consider the operator equation

$$i\partial W(t)/\partial t=H(t)W(t) \tag{4}$$

and its hermitian adjoint

$$i\partial\bar{W}/\partial t=-\bar{W}(t)H(t). \tag{5}$$

$H(t)$ is assumed to be hermitian. Two physically interesting implicit solutions of (4) are

$$U^r(t)=1-i\int_{-\infty}^{t}dt'H(t')U^r(t') \tag{6r}$$

$$U^a(t)=1-i\int_{+\infty}^{t}dt'H(t')U^a(t'). \tag{6a}$$

The solution $U^r(t)$ is to be identified with the $U(t)$ mentioned in the introduction, but the symbol $U(t)$ without a superscript will henceforth refer to both $U^r(t)$ and $U^a(t)$. The corresponding solutions of (5) are the hermitian adjoints of (6). An identity:

$$i\frac{\partial}{\partial\tau}[\bar{U}(\tau)-1][U(\tau)-1]=\bar{U}(\tau)H(\tau)-H(\tau)U(\tau) \tag{7}$$

constructed from (4) and (5), is now integrated between $-\infty$ and t for $U^r(t)$ and between $+\infty$ and t for $U^a(t)$. This operation yields directly

$$\bar{U}(t)U(t)=1 \tag{8}$$

and in the limit as $t\pm\infty$,

$$\bar{S}^rS^r=1;\quad \bar{S}^aS^a=1. \tag{9r, a}$$

Equations 8 and 9 are not sufficient to insure (1) or (2). Statement (2) can, however, be deduced from another identity. We integrate

$$i\frac{\partial}{\partial\tau}[\bar{U}^r(\tau)-1][U^a(\tau)-1]=\bar{U}^r(\tau)H(\tau)-H(\tau)U^a(\tau) \tag{10}$$

between the limits $-\infty$ and $+\infty$. This leads to an expression

$$\bar{S}^r=S^a \tag{11}$$

or together with (9)

$$S^r\bar{S}^r=1;\quad S^a\bar{S}^a=1. \tag{12r, a}$$

Relations (12) and (9) then imply (2). Equation (10) integrated between $-\infty$ and a finite time t gives in conjunction with (11)

$$S^r=\bar{U}^a(t)U^r(t) \tag{13r}$$

$$S^a=\bar{U}^r(t)U^a(t), \tag{13a}$$

which may be taken as the defining equations for S^r and S^a even if the limits $U^r(+\infty)$, $U^a(-\infty)$ do not properly exist.[1]

A somewhat better insight into the nature of these relations is gained by connecting $U^r(t)$, $U^a(t)$ with another special solution of (4):

$$U^s(t)=1-\frac{i}{2}\int_{-\infty}^{+\infty}dt'\epsilon(t-t')H(t')U^s(t') \tag{14}$$

where $\epsilon(x)$ denotes the signum function of x. The operator $U^s(t)$ may be used to construct the Cayley representation of S.[2] Its essential properties,

$$\bar{U}^s(t)U^s(t)=\bar{U}^s(\infty)U^s(\infty)=\bar{U}^s(-\infty)U^s(-\infty) \tag{15}$$

$$\int_{-\infty}^{+\infty}dt'H(t')U^s(t')=\int_{-\infty}^{+\infty}dt'\bar{U}^s(t')H(t') \tag{16}$$

readily follow from the integration of the identity

$$i\frac{\partial}{\partial\tau}[\bar{U}^s(\tau)-1][U^s(\tau)-1]=\bar{U}^s(\tau)H(\tau)-H(\tau)U^s(\tau) \tag{17}$$

and its product with $\epsilon(t-\tau)$ between the limits $-\infty$ and $+\infty$. The relations we are interested in are obtained from

$$i\frac{\partial}{\partial\tau}[\bar{U}^s(\tau)-1][U(\tau)-1]=\bar{U}^s(\tau)H(\tau)-H(\tau)U(\tau) \tag{18}$$

when this is integrated over the interval $(-\infty, t)$ for $U(t)=U^r(t)$ and $(+\infty, t)$ for $U(t)=U^a(t)$.

With the aid of (16) we then get[3]

$$\bar{U}^s(t)U^r(t)=U^s(\infty) \tag{19r}$$

$$\bar{U}^s(t)U^a(t)=\bar{U}^s(\infty). \tag{19a}$$

A sufficient condition for the unitarity of $U(t)$ is now seen to be the existence of $[U^s(t)]^{-1}$ in the sense of a right inverse. In that case

$$U^r(t)=[\bar{U}^s(t)]^{-1}U^s(\infty) \tag{20r}$$

$$U^a(t)=[\bar{U}^s(t)]^{-1}\bar{U}^s(\infty) \tag{20a}$$

and

$$\begin{aligned}U^r(t)\bar{U}^r(t)&=[\bar{U}^s(t)]^{-1}U^s(\infty)\bar{U}^s(\infty)[U^s(t)]^{-1}\\&=[\bar{U}^s(t)]^{-1}\bar{U}^s(t)U^s(t)[U^s(t)]^{-1}\\&=1.\end{aligned} \tag{21}$$

The transition from the second to the third member of (21) involved the use of

$$\bar{U}^s(\infty)U^s(\infty)=U^s(\infty)\bar{U}^s(\infty) \tag{22}$$

which is an immediate consequence of (16). The reciprocal of $U^s(t)$ will exist in general only in the limit $t\to\pm\infty$ when the operator $i[U^s(t)-1]$ becomes hermitian on account of (16). In this limit (20) leads to the Cayley representations of S^r and S^a as given in reference 2. A unitary $U(t)$ can however always be expressed in the form

$$U^r(t)=U^s(t)[\bar{U}^s(\infty)]^{-1} \tag{23r}$$

$$U^a(t)=U^s(t)[U^s(\infty)]^{-1} \tag{23a}$$

since the reciprocal of $U^s(\infty)$ is known to exist on account of (16).

The hermiticity of $i[U^s(t)-1]$, even though sufficient, is by no means necessary to insure the unitarity of $U(t)$. To see this we assume that $i[U^s(t)-1]$ is anti-hermitian and show that in this case too $U(t)$ is a unitary operator. Starting from (15) we have

$$\begin{aligned}\bar{U}^s(\infty)U^s(\infty)&=U^s(t)U^s(t)=\bar{U}^r(t)U^s(t)U^s(t)U^r(t)\\&=\bar{U}^r(t)\bar{U}^s(\infty)U^s(\infty)U^r(t)\\&=\bar{U}^r(t)U^s(t)U^a(t)\bar{U}^a(t)U^s(t)U^r(t)\\&=\bar{U}^s(\infty)U^a(t)\bar{U}^a(t)U^s(\infty).\end{aligned} \tag{24}$$